Improved thermoelectric properties of nanostructured composites out of Bi$_{1-X}$Sb$_X$ nanoparticles and carbon phases

Ekrem $_{Güneş}$, Mathias S. Wickleder, Eckhard Müller, Matthias T. Elm 🆔, and Peter J. Klar

View Online   Export Citation   CrossMark

ARTICLES YOU MAY BE INTERESTED IN

Improved thermoelectric properties of nanostructured composites out of Bi$_{1-x}$Sb$_x$ nanoparticles and carbon phases

Ekrem Güneş,[1,2] Mathias S. Wickleder,[1] Eckhard Müller,[3,4]
Matthias T. Elm,[4,5,6] and Peter J. Klar[4,5,a]

[1]*Institute of Inorganic and Analytical Chemistry, Justus-Liebig University,
Giessen D-35392, Germany*
[2]*Department of Alternative Energy Resources, Harran University, Şanlıurfa TR-63300, Turkey*
[3]*Center for Materials Research, Justus-Liebig University, Giessen D-35392, Germany*
[4]*Institute of Materials Research, German Aerospace Center (DLR), Kön D-51170, Germany*
[5]*Institute of Experimental Physics I, Justus-Liebig University, Giessen D-35392, Germany*
[6]*Institute of Physical Chemistry, Justus-Liebig University, Giessen D-35392, Germany*

Thermoelectric figures of merit of $ZT \approx 0.4$ at room temperature were achieved in nanostructured composite materials prepared by uniaxial pressing of Bi$_{1-x}$Sb$_x$ nanoparticles and 0.3 wt.% of a carbon phase. This constitutes a significant improvement of the low-temperature thermoelectric material Bi$_{1-x}$Sb$_x$ and strongly suggests the possibility of employing these materials in efficient thermoelectric devices working at room temperature. Interestingly, the beneficial effect of the carbon phase added to nanostructured Bi$_{1-x}$Sb$_x$ is the same for either carbon nanotubes or active carbon. This finding is attributed, on the one hand, to a combination of electronic band gap engineering due to nanostructuring and energy filtering due to graphene-like interlayers between Bi$_{1-x}$Sb$_x$ grains and, on the other hand, to modified phonon scattering at the grain boundaries and additional phonon scattering by agglomeration sites of carbon material on the μm scale. © *2018 Author(s). All article content, except where otherwise noted, is licensed under a Creative Commons Attribution (CC BY) license (http://creativecommons.org/licenses/by/4.0/).* https://doi.org/10.1063/1.5034525

I. INTRODUCTION

The growing demand of energy and the society's awareness of environmental issues such as global warming constitute driving forces for tapping renewable energy sources such as sun light or wind instead of fossil fuels,[1,2] but also for improving the efficiency of existing energy conversion processes.[3–5] Thermoelectric generators possess the potential of converting an additional fraction of the large amounts of unused waste heat of combustion processes in automobiles, industrial plants, and other facilities into electricity and thus to diminish these losses. However, the still rather low efficiency of thermoelectric generators restricts a wide and economically viable application. The efficiency of the thermoelectric generator depends largely on the dimensionless thermoelectric figures of merit of the materials employed in its p-type and n-type legs. The thermoelectric figure of merit ZT of a material is defined as $ZT = \sigma S^2 T / \kappa$ where σ, S, and κ denote the electrical conductivity, the Seebeck coefficient, and thermal conductivity, respectively. Best conventional thermoelectric bulk materials barely reach a ZT of 1; values of at least 2 need to be targeted for thermoelectric technologies to become of interest on a mass market scale.[6] Different strategies are currently pursued in the quest for materials with a higher ZT.[6–9] A promising strategy is to employ hybrid structures where the thermoelectric properties are tuned by combining two constituents. If the hybrid formation takes place on the nanoscale or mesoscale, it will often be found that the resulting thermoelectric

---

[a]Electronic address: peter.j.klar@exp1.physik.uni-giessen.de

properties deviate significantly from those predicted by effective medium theory.[10,11] This finding indicates that the interfaces between the constituents play a significant role in the transport processes of charge carriers and phonons determining the transport coefficients σ, S, and κ.[12] For example, hybrid materials may be obtained by thermally induced segregation of nanoinclusions in a bulk material or by mixing nanostructures of different origin and compacting the mixture by hot or cold pressing. The latter approach yields more degrees of freedom as the various nanostructures combined can be chosen more or less freely in terms of composition and morphology. Carbon nanotubes (CNT) are often chosen as one constituent of such hybrid materials due to their unusual mechanical, thermal and electrical properties.[10,18–23] We have recently demonstrated that nanostructured composites of CNT and $Bi_{1-x}Sb_x$ nanoparticles exhibit considerably improved thermoelectric properties.[24] Here, we show that nanostructured composites of active carbon (AC) and $Bi_{1-x}Sb_x$ nanoparticles exhibit similar thermoelectric properties than the original $Bi_{1-x}Sb_x$/CNT composites. These findings implies that the improvement of the thermoelectric properties of $Bi_{1-x}Sb_x$/CNT composites is not related to the tubular structure of CNT or a resulting CNT network interpenetrating the nanostructured $Bi_{1-x}Sb_x$ but rather to carbon-related modifications of the interfaces between the $Bi_{1-x}Sb_x$ nanoparticles.

II. EXPERIMENTAL DETAILS

$Bi_{1-x}Sb_x$ nanoparticles with x = 0.1, 0.12, 0.13, 0.15, and 0.2 were synthesized by ball-milling of powders of the elemental constituents (bismuth: 99.5% Alfa Aesar; antimony: 99.5% Roth). For this, the weighed amounts of the powders were transferred into a stainless steel milling container and sealed under argon atmosphere. It followed a twenty-hour ball-milling procedure using a ball-powder-ration of 7.5: 1 and 450 revolutions per minute (rpm). After ball-milling the powders were removed under inert gas and subsequently transferred into a Schlenk tube, where they were tempered for 17 hours at 250 °C under a gentle argon stream.[17,24,25] A detailed characterization of the $Bi_{1-x}Sb_x$ nanoparticles can be found in Ref. 24. In brief, the $Bi_{1-x}Sb_x$ nanoparticles were crystalline, alloy formation took place, and the nanoparticles were between 50 nm and 100 nm in diameter. After synthesis, the $Bi_{1-x}Sb_x$ matrix material was mixed with 0.3 wt.% of either CNT (Baytubes C70P) or AC (Merck Millipore). Weighing of the educts was realized under argon atmosphere. A content of 0.3 wt.% of the carbon phase was chosen because $Bi_{1-x}Sb_x$/CNT composites with 0.3 wt.% of CNT were found to be less brittle than composites with higher CNT contents and already showed a *ZT* enhancement by a factor of about 2.5 compared to the reference samples without CNT.[24] The mixtures were pressed for two hours at a pressure of 780 MPa at 50 °C to form pellets of cylindrical shape. After the pressing the samples were pestled and pressed again to achieve a high degree of homogeneity. The second pressing step lasted for three hours using the same pressing conditions (50 °C, 780 MPa). For all five compositions x and both carbon materials, we prepared two pellets of different shape to enable us to determine all three transport coefficients along the y-direction, i.e. perpendicular to uniaxial pressing direction z. In Ref. 24, we reported an anisotropy of the transport properties of the nanostructured $Bi_{1-x}Sb_x$/CNT composites introduced by the uniaxial pressing procedure. There, it turned out that the *ZT* values of the composite samples obtained for transport along the y-direction were superior to those found for transport along z. The pellets were tempered for 17 hours at 250 °C to ensure the recovery and relaxation of the material from the mechanical strain caused by the pressing process. In addition, we prepared nanostructured $Bi_{1-x}Sb_x$ reference samples for all five compositions.

III. RESULTS AND DISCUSSION

A. Characterization of the microstructure

The microstructure of the $Bi_{1-x}Sb_x$/CNT and $Bi_{1-x}Sb_x$/AC composites as well as of the $Bi_{1-x}Sb_x$ reference samples was further investigated using scanning electron microscopy (SEM, JEOL JSM 7001F) with an acceleration voltage of 15 keV. Figure 1 shows typical SEM images of the three kinds of samples. Figure 1(a) shows that the pellet surface of the reference samples is smooth and dense down to the 1 μm scale. High compactness with only a low degree of microstructural defects from the
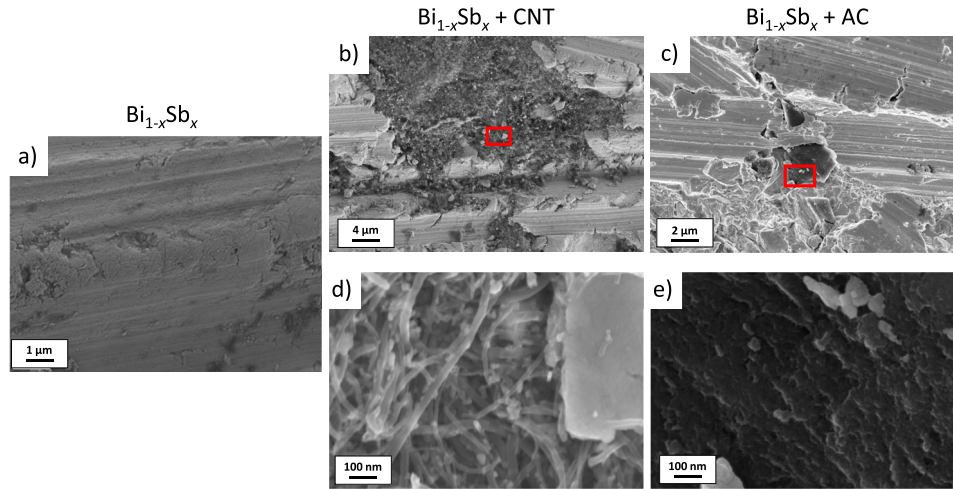
FIG. 1. (a) SEM-image of the surface of a pellet prepared from $Bi_{1-x}Sb_x$ nanoparticles alone. (b) and (d) SEM-images of the surface of a pellet of a $Bi_{1-x}Sb_x$/CNT composite at two different magnifications. (c) and (e) SEM-images of the surface of a pellet of a $Bi_{1-x}Sb_x$/AC composite at two different magnifications. Figures (d) and (e) show the marked region in Figures (b) and (c).

millimeter scale down to the micrometer scale is found for all reference samples. Images of pellets of $Bi_{1-x}Sb_x$/CNT and $Bi_{1-x}Sb_x$/AC composites are shown in Figs. 1(b) and (c), respectively, and demonstrate a similar level of compactness from the millimeter down to 100 μm scale. However, both images also reveal isolated structural defects on the 1 μm scale which in both cases correspond to agglomerations of the carbon materials. Figs. 1(d) and (e) are close views of higher magnification of such agglomerations and show the interconnected CNT bundles and layered AC material, respectively. Thus, the microstructure of the inclusion materials is to a large extent preserved at these agglomeration sites. As the agglomeration sites are separated by μm distances and thus do not form a close network pervading the entire composite sample their impact on the electronic transport properties should be rather weak. This is in accordance with the temperature-dependent magneto-transport results reported for the $Bi_{1-x}Sb_x$/CNT composites in Ref. 24 which are very similar to those of the $Bi_{1-x}Sb_x$ reference samples and can be consistently explained by temperature, composition and confinement-induced changes of the $Bi_{1-x}Sb_x$ band structure.[14–16] However, the agglomeration sites may act as scattering centers for phonons with small wave vectors.

B. Characterization of the thermoelectric properties

Magneto-transport measurements were performed in the temperature range between 30 and 300K using a superconducting magnet system (Oxford) generating magnetic fields up to 10T. The electrical conductivity was measured in van der Pauw geometry with indium contacts soldered onto the sample surface and with the magnetic field applied perpendicular to the sample surface. The thermal conductivity was determined from the thermal diffusivity measured using a Linseis XFA (Linseis, Selb Germany). The Seebeck coefficient was determined between 120 and 310K using a custom-made setup. Between 300 and 473K the Seebeck coefficient and the electrical conductivity were measured simultaneously in four-point geometry using a LSR-3 device (Linseis, Selb Germany). All transport coefficients of the composites were measured along the *y*-direction. Figure 2 summarizes the room-temperature thermoelectric properties of the three types of samples. As a trend, incorporation of the carbon material increases the electrical conductivity σ, increases the absolute value of the Seebeck coefficient *S*, but decreases the thermal conductivity κ, leading to a rise of the *ZT* value at room temperature from about 0.15 for conventional crystalline material to about 0.4 as shown in Fig. 3d).[13,24] This is about half the room-temperature *ZT* value of that of Bi_2Te_3 based materials which are currently employed in thermoelectric devices used at temperatures close to room temperature.[26,27] It should be noted that the *ZT* values obtained are within the experimental uncertainty independent of the type of carbon material used. In particular, we can rule out that the *ZT* enhancement observed
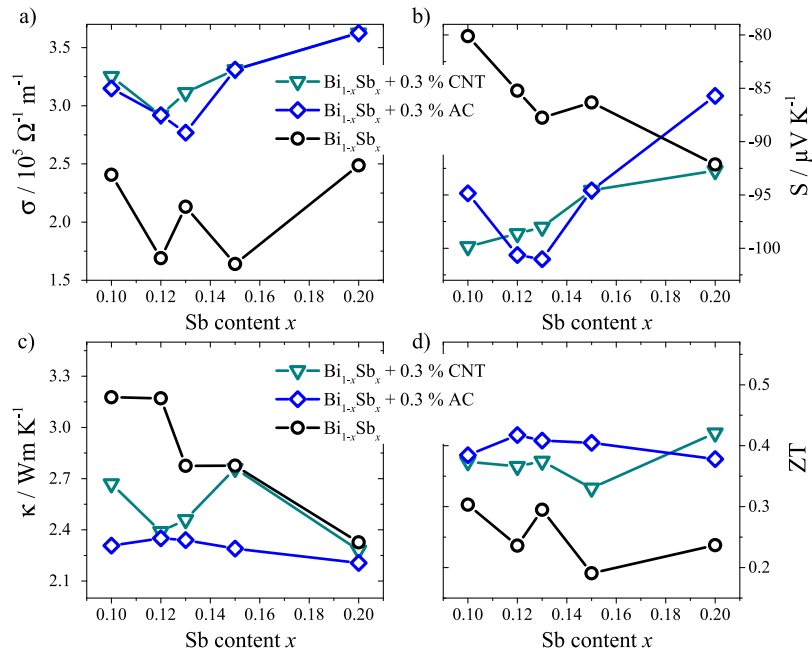
FIG. 2. Room-temperature thermoelectric properties of $Bi_{1-x}Sb_x$/CNT (triangles) and $Bi_{1-x}Sb_x$/AC composites (diamonds) as well as of the nanostructured $Bi_{1-x}Sb_x$ reference samples (circles); a) electrical conductivity, b) Seebeck coefficient, c) thermal conductivity, and d) Figure of Merit.

in the two series of composite samples is related to the special mechanical, thermal and electrical properties of CNTs as AC possesses an entirely different morphology, but yields similar results. Furthermore, all three series of samples exhibit negative Seebeck coefficients at room temperature. Thus, the electronic transport of the nanostructured composites as well as of the nanostructured
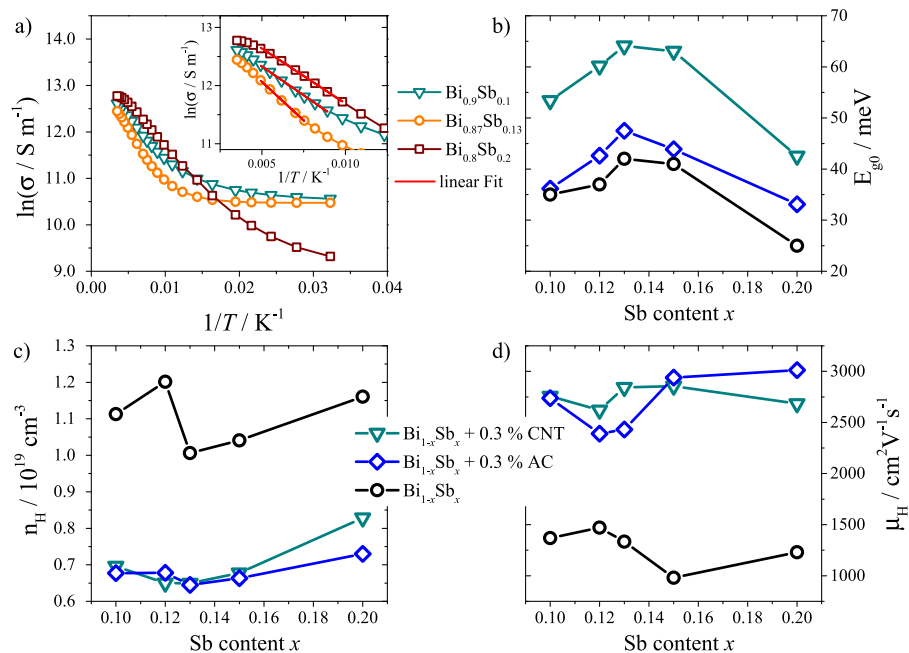

FIG. 3. (a) Temperature dependence of the electrical conductivity of the nanostructured $Bi_{1-x}Sb_x$/AC composites. The inset shows the linear fit in the temperature from 100 to 200K. b) Thermal band gaps, c) effective carrier concentration, and d) Hall mobility of $Bi_{1-x}Sb_x$/AC, $Bi_{1-x}Sb_x$/CNT, and nanostructured $Bi_{1-x}Sb_x$ reference samples.

reference material is dominated by high-mobility electrons excited across the small band gap at this temperature. This finding is further corroborated by the results shown in Fig. 3.

Figure 3 summarizes the results of the low-temperature transport measurements. As an example, Fig. 3(a) displays temperature-dependence of the electrical conductivity of the $Bi_{1-x}Sb_x$/AC composites. The temperature-dependence observed is typical for BiSb alloys.[16,24,25] At low temperatures a nearly constant conductivity is found, which is due to the formation of an impurity band caused by impurities in the reactants used in the synthesis process. With increasing temperature the conductivity increases revealing a semiconducting behavior. At temperatures above 300K the composites exhibit a metal-like behavior due to their small band gap, where the decrease in conductivity can be attributed to increasing phonon scattering. In the semiconducting temperature range (100K to about 200K) the thermal band gaps of the composites were estimated from the slope of a linear fit in an Arrhenius representation of the conductivity (inset in Fig. 3a)). The thermal band gaps determined for the two series of composite samples as well as for the nanostructured reference samples are shown in Fig. 3b). For all three series, a maximum of the thermal band gap occurs for an Sb content of about 12 to 13% as known for bulk $Bi_{1-x}Sb_x$ alloys. Thus, the inclusion of carbon material has no significant effect on the composition dependence of the band structure of the nanostructured matrix material, but it changes the magnitude of the band gaps, i.e. leads to a stronger confinement of the electronic states in the $Bi_{1-x}Sb_x$ nanoparticles forming the samples. The effective carrier concentration n_H (Fig. 3c)) as well as the Hall mobility μ_H (Fig. 3d)) were extracted from the magneto-transport data at high magnetic fields assuming a simple Drude model, i.e. the ambipolar transport properties of $Bi_{1-x}Sb_x$ alloys[15,16,28] were neglected. Thus, the values obtained only represent an effective carrier concentration and somewhat correspond to the difference between majority and minority carriers in the different bands. In all samples, electrons are the majority carriers at room temperature due to the small band gap and higher mobilities compared to holes. The behavior of the effective carrier concentration is almost the same for all three series of samples and can mainly be attributed to the changes of the band structure with Sb content. With increasing thermal band gap, i.e. increasing Sb content, the carrier concentration decreases reaching a minimum for an Sb content of about 13%, where the largest band gap is observed in each series. The reduction of the thermal band gap observed at higher Sb content again correlates with a rise of the effective carrier concentration. Furthermore, when comparing the mobility values of the two series of composite samples to those of the nanostructured reference material a significant enhancement of the mobility values in the composites is found. The beneficial effect of the carbon inclusion on the mobilities of the majority charge carriers may be attributed to graphene-like abrasion products formed during the pestling.[24] These products can form a carbon coating on the single $Bi_{1-x}Sb_x$ surface which may act as energy barriers between the grains. Then, low energy electrons cannot pass the energy barriers resulting in an energy filtering effect and thus in a significant increase of the mobility of the charge carriers due to reduced electron-electron scattering.[29–32] In a simple model the Seebeck coefficient depends reciprocal on the carrier concentration.[33] This correlation between Seebeck coefficient and carrier concentration (i.e. band gap) is reflected in the composition dependence of the Seebeck coefficient at 300K for all three series of samples investigated. Maxima of the thermal band gap as a function of composition x are found close to an Sb content of 13 %, where the samples possess the lowest effective carrier concentrations and correspondingly exhibit the highest absolute values of the Seebeck coefficient. Energy filtering not only increases the mobility of the charge carriers, but also reduces the effective carrier concentration.[29] Thus, the larger absolute values of the Seebeck coefficients in conjunction with lower effective carrier concentrations in the composites compared to the reference samples support the assumption of a carbon-like layer between the $Bi_{1-x}Sb_x$ nanoparticles of the composites. The inclusion of carbon materials in the composites also results in a remarkable reduction of κ for all compositions investigated. Especially for low Sb content a reduction of the thermal conductivity of about 25% is observed. The modification of the boundaries between the $Bi_{1-x}Sb_x$ nanoparticles by carbon is likely to contribute to this effect. However, the variation of the content of the carbon phase in the composite also revealed a correlation between the density of the agglomeration sites and the reduction of the thermal conductivity. Thus, we believe that the existence of the agglomeration sites, which act as additional scattering centers for phonons, also contributes to the reduction of κ observed in the composites.

IV. SUMMARY

Nanostructured composite materials prepared by compacting mixtures of $Bi_{1-x}Sb_x$ nanoparticles with carbon phases such as CNT or AC possess thermoelectric properties superior to those of the nanostructured $Bi_{1-x}Sb_x$ reference samples. The thermoelectric properties of $Bi_{1-x}Sb_x$/CNT and $Bi_{1-x}Sb_x$/AC composites with the same mass fraction of the carbon phase are very similar despite the morphological differences between CNT and AC. The experimental data can be consistently explained by the formation of carbon-like layers between the $Bi_{1-x}Sb_x$ nanoparticles of the composites accompanied by the formation of agglomeration sites of the carbon material on the μm scale. The modification of the grain boundaries by carbon leads to energy filtering effects which are advantageous for the electronic transport coefficients and possibly reduce the thermal conductivity. The agglomeration sites add another contribution to the reduction of the thermal conductivity by acting as additional scattering centers for phonons. As the morphology or dimensionality of the carbon inclusion material (CNT vs. AC) is not important, active carbon represents a cheap alternative to carbon nanotubes for tuning the micro- and nanostructural properties of these thermoelectric composite materials. Furthermore, the significant increase of *ZT* value by almost a factor of 3 may establish nanostructured $Bi_{1-x}Sb_x$/AC composites as thermoelectric materials also for room temperature applications. More importantly, the *ZT* values achieved are about half of the room-temperature *ZT* value of Bi_2Te_3 bulk material which is currently employed in thermoelectric devices for applications close to room temperature.

[1] J. Khan and M. H. Arsalan, Renewable and Sustainable Energy Rev. **55**, 414 (2016).
[2] Y. Kumar, J. Ringenberg, S. S. Depuru, V. K. Devabhaktuni, J. W. Lee, E. Nikolaidis, B. Andersen, and A. Afjeh, Renewable and Sustainable Energy Rev. **53**, 209 (2016).
[3] L. E. Bell, Science **321**, 1457 (2008).
[4] S. Schlecht and H. Böttner, Nachr. Chem. **56**, 136 (2008).
[5] A. J. Minnich, M. S. Dresselhaus, Z. F. Ren, and G. Chen, Energy Environ. Sci. **2**, 466 (2009).
[6] C. J. Vineis, A. Shakouri, A. Majumdar, and M. G. Kanatzidis, Adv. Mater. **22**, 3970 (2010).
[7] J. R. Sootsman, D. Y. Chung, and M. G. Kanatzidis, Angew. Chem. **121**, 8768 (2009).
[8] G. F. Snyder and E. S. Toberer, Nature Mater. **7**, 105 (2008).
[9] M. G. Kanatzidis, Chem. Mater. **22**, 648 (2010).
[10] R. Nunna, P. Qiu, M. Yin, H. Chen, R. Hanus, Q. Song, T. Zhang, M.-Y. Chou, M. T. Agne, J. He, G. F. Snyder, X. Shi, and L. Chen, Energy Environ. Sci. **10**, 1928 (2017).
[11] M. T. Elm, T. Henning, P. J. Klar, and B. Szyszka, Appl. Phys. Lett. **93**, 232101 (2008).
[12] F. Gather, C. Heiliger, and P. J. Klar, Prog. Solid State Chem. **39**, 97 (2011).
[13] G. E. Smith and R. Wolfe, J. Appl. Phys. **33**, 841 (1962).
[14] P. W. Chao, H. T. Chu, and Y. H. Kao, Phys. Rev B **9**, 4030 (1974).
[15] G. Oelgart, G. Schneider, W. Kraak, and R. Herrmann, Phys. Stat. Sol.(b) **74**, K75 (1976).
[16] C. H. Will, M. T. Elm, P. J. Klar, B. Landschreiber, E. Güneş, and S. Schlecht, J. Appl. Phys. **114**, 193707 (2013).
[17] B. Landschreiber, E. Güneş, C. Rohner, G. Homm, C. Will, A. Sesselmann, P. J. Klar, E. Müller, and S. Schlecht, AIP Conf. Proc. **1449**, 303 (2012).
[18] G.-D. Zhan, J. D. Kuntz, A. K. Mukherjee, P. Zhu, and K. Koumoto, Scr. Mater. **54**, 77 (2006).
[19] C. Meng, C. Liu, and S. Fan, Adv. Mater. **22**, 535 (2010).
[20] Q. Yao, L. Chen, W. Zhang, S. Liufu, and X. Chen, ACS Nano **4**, 2445 (2010).
[21] C. Yu, Y. S. Kim, D. Kim, and J. C. Grunlan, Nano Letters **8**, 4428 (2008).
[22] K. Zhang, Y. Zhang, and S. Wang, Sci. Rep. **3**, 3448 (2013).
[23] F. Ren, H. Wang, P. A. Menchhofer, and J. O. Kiggans, Appl. Phys. Lett. **103**, 221907 (2013).
[24] E. Güneş, F. Gundlach, M. T. Elm, P. J. Klar, S. Schlecht, M. S. Wickleder, and E. Müller, ACS Appl. Mater. Interfaces **9**, 44756 (2017).
[25] E. Güneş, B. Landschreiber, D. Hartung, M. T. Elm, C. Rohner, P. J. Klar, and S. Schlecht, J. Electron. Mater. **43**, 2127 (2014).
[26] S. Scherrer, H. Scherrer, and D. M. Rowe, *CRC Handbook of Thermoelectrics* (CRC Press, 1995).
[27] Y. Wu, R. Zhai, T. Zhu, and X. Zhao, Mater. Today Phys. **2**, 62 (2017).
[28] B. Lenoir, M. Cassart, J. P. Michenaud, H. Scherrer, and S. Scherrer, J. Phys. Chem. Solids **57**, 89 (1996).
[29] J. P. A. Makongo, D. K. Misra, X. Zhou, A. Pant, M. R. Shabetai, X. Su, C. Uher, K. L. Stokes, and P. F. P. Poudeu, J. Am. Chem. Soc. **133**, 18843 (2011).
[30] Y. Nishio and T. Hirano, Jpn J. Appl. Phys. **36**, 170 (1997).
[31] B. Paul, V. A. Kumar, and P. Banerji, J. Appl. Phys. **108**, 064322 (2010).
[32] A. Soni, Y. Shen, M. Yin, Y. Zhao, L. Yu, X. Hu, Z. Dong, K. A. Khor, M. S. Dresselhaus, and Q. Xiong, Nano Lett. **12**, 4305 (2012).
[33] M. Cutler, J. F. Leavy, and R. L. Fitzpatrick, Phys. Rev. **133**, A1143 (1964).